MODELING OF THE GENERAL CIRCULATION WITH THE LMD-AOPP-IAA GCM: UPDATE ON MODEL DESIGN AND COMPARISON WITH OBSERVATIONS .

F. Forget, M. Angelats i Coll, Y. Wanherdrick, F. Hourdin, *Laboratoire de Meteorologie Dynamique du CNRS, Paris, France***, S. Lewis, P. Read, F. Taylor,** *atmospheric, Oceanic and Planetary Physics, Univ. of Oxford, Oxford OX1 3PU, UK***, M. Lopez-Valverde, M. Lopez-Puertas,** *Instituto de Astrofisica de Andalucia, 18080 Granada, Spain***.**

I. The LMD-AOPP GCM

The LMD-AOPP GCM is developed conjointly by LMD in Paris and AOPP in Oxford, with the collaboration of IAA in Granada for the physical processes specific to the upper atmosphere. The collaboration between the two teams is based on the use of two different dynamical core (grid-point at LMD, spectral at AOPP), which allow us to estimate the likely uncertainty arising from certain types of modeling errors. Similarly, we use different scheme to compute tracer transport, etc... The work has benefited from support from ESA (since 1995) and CNES (since 2000). Within that context, the GCMs are used to produce a Martian climate "database" which is used by more than 30 teams around the world for mission design and scientific studies (see Bingham et al., this issue and Lewis et al., 1999).

The baseline version of the GCM is described in detail in Forget et al. (1999). Here we describe the recent improvement and design changes since this publication. Compared to this previous version, the new GCM covers a wider range of altitude, from 0 to 120 km in the vertical, it uses improved topography and thermal inertia surface maps from Mars Global Surveyor (MGS), and includes a new "dust scenario" to describe the distribution of airborne dust in the atmosphere.

Surface fields

The topography now used by the model is, of course, the topography measured by MOLA aboard Mars Express. New thermal inertia data deduced from MGS TES have been retrieved by Mellon et al. (2000) and included in th GCM. However, this paper only provided reliable measurements from 65°North to about 30°South, and no global map has been released so far. Therefore, for the rest of the planet, we continue to use the canonic thermal inertia map from Palluconi and Kieffer (1981) extended to the polar region by Paige et al. (1994) and Paige and Keegan (1994). However, on the basis of the analyses performed by Haberle and Jakosky (1991) and Hayashi et al. (1995) regarding the impact of the airborne dust on thermal inertia (not properly accounted in these less recent analyses), we have applied some correction to the old dataset: 1) between 90°N and 65°N, the Paige et al. (1994) data are decreased by 25%, 2) Between 30°S and 60°S, the Palluconi and Kieffer (1981) data are decreased by 8% 3) Between 60°S and 90°S Paige and Keegan (1994) data are decreased by 28%. These corrections yield an homogeneous dataset , and are shown to be consistent with the impact of the dust when the measurements were made.

A new "dust scenario"

The distribution of dust is highly variable on Mars. Although we have developed dedicated version of the model to simulate the dust cycle and predict interactive dust fields, for most application, the amount of dust in the atmosphere must be prescribed. In order to roughly match the thermal structure of the atmosphere observed by MGS at the beginning of the mission (TES and radio occultation), we found necessary to vary the prescribed amount of dust in the atmosphere as a function of altitude, latitude, and season. In practice, the dust optical depth (defined at 700 Pa) and the dust vertical distribution is varried using simple sinusoidal functions. The corresponding spatial and temporal evolutions are represented on Figure 1. This "dust scenario" is now used for our baseline simulations and most applications were we wish to represent a "typical martian year".

Vertical extension up to 120 km

Motivation. The atmosphere of Mars above 70 km remain poorly known. On the one hand, very little observations have been obtained by remote sensing instruments. Only a few in-situ measurements are available, including the 3 density profiles from the Viking and Pathfinder entries and the density measurements obtained during the aerobraking phases of the MGS and Mars oddyssey missions. On the other hand, very little comprehensive GCM studies have been performed in the 70-120km altitude range. This is due to the fact that the GCMs cannot accurately be used above 80 km because the Local Thermal Equilibrium (LTE) assumed in these models to compute the radiative heating and cooling budget of the atmosphere is not valid at such low pressures.

The few observations available (in-situ density observations) have revealed a very interesting middle atmosphere with a complex and highly variable dynamics combining various kind of waves probably interacting with the mean circulation (Keating et al., 1998 ; Magalhães et al. 1999). Moreover, information on this part

of the atmosphere is vital to prepare spacecraft missions performing aerobraking, aerocapture or re-entry.

Parameterization of non-LTE Near Infrared CO_2 solar heating. The main impact of non-LTE processes on the solar heating rates is that a significant fraction of the solar energy absorbed in the 2.7 and 4.3 μm regions is emitted back to space (10% at 80 km, 50% at 100 km, 80% at 107 km), mostly at other vibrational levels, instead of heating the gas as it would happen in LTE conditions. Detailed calculations of the actual solar heating rate using a full non-LTE model including 92 transitions have been performed by Lopez-Puertas and Lopez-Valverde (1995, see also reference therein) and Lopez-Valverde et al. (1998). Fortunately, the solar absorption in the near-infrared is only weakly dependent on the thermal structure of the atmosphere. This allowed Lopez-Valverde et al. (1998) to provide a table of correction factors on a pressure grid to convert LTE radiative transfer calculation heating rate into realistic heating rates. On this basis, we have updated the function used in Forget et al. (1999) to accurately compute the near Infrared CO_2 solar absorption at high altitude. At pressure $p_0 = 700$ Pa and for a mean Mars-Sun distance $r_0 = 1.52$ AU, the heating rate (per martian day) corresponding to a zero solar zenith angle ($\mu = 0$) is taken to be $\partial T/\partial t(p_0, r_0, 0) = 1.1956$ K day^{-1} The heating rate at other pressures p, Mars-Sun distance r, and zenithal angle μ is then computed as follows:

$$\frac{\partial T}{\partial t}(p, r, \mu) = \frac{\partial T}{\partial t}(p_0, r_0, 0) \times \frac{r_0^2}{r^2} \sqrt{\frac{p_0}{p}} \tilde{\mu} \left(1 + \frac{p_1}{p}\right)^{-b} \quad (1)$$

with $p_1 = 0.0015889$ Pa, $b = 1.9628$ and $\tilde{\mu}$ the cosine of the solar zenith angle corrected for atmospheric refraction (we use $\tilde{\mu} = [(1224\mu^2 + 1)/1225)]^{1/2}$).

Parameterization of non-LTE thermal cooling rate. Unfortunately, a simple scheme similar to the one used at solar wavelengths is not possible for the thermal cooling rates which are strongly affected by the varying thermal structure (Lopez-Puertas and Lopez-Valverde, 1995). In theory, it would be necessary to take into accounts the evolution of tens of transitions between the various internal energy mode (fundamentals, hot bands), for various isotopes, as performed in the full IAA model. This is much too computationally expensive for a GCM. Nevertheless, after investigating various method to simplify the problem, a new parameterization have been developped for the GCM. This non-LTE thermal infrared model is well adapted to the upper atmosphere where non-LTE processes occurs but remain crude below. to compute the cooling rate at any level in the GCM, we merge the non-LTE cooling rate results with the cooling rate computed by the more sophisticated GCM orginal LTE wide band model.
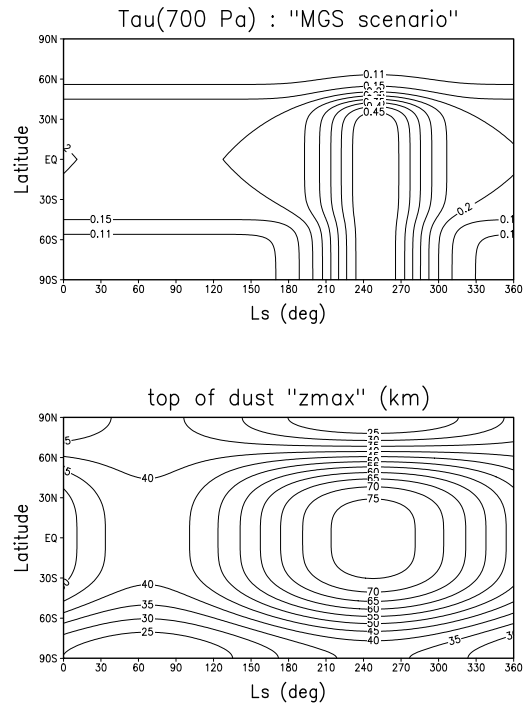

Figure 1: Our baseline "MGS dust scenario": Variation of the reference optical depth τ at 700 Pa and the altitude of the top of the dust layer z_{max} as a function of season (solar longitude L_s) and latitude. The dust mass mixing ratio q is defined as a function of pressure p; that is, $q = q_0 \exp\left\{0.007 \left[1 - (p_0/p)^{(70\ km/z_{max})}\right]\right\}$ where where q_0 is a constant determined by the prescribed optical depth.

Winds at p= 0.47 Pa (65km) (Ls=0−30 ; noon at lon=0)

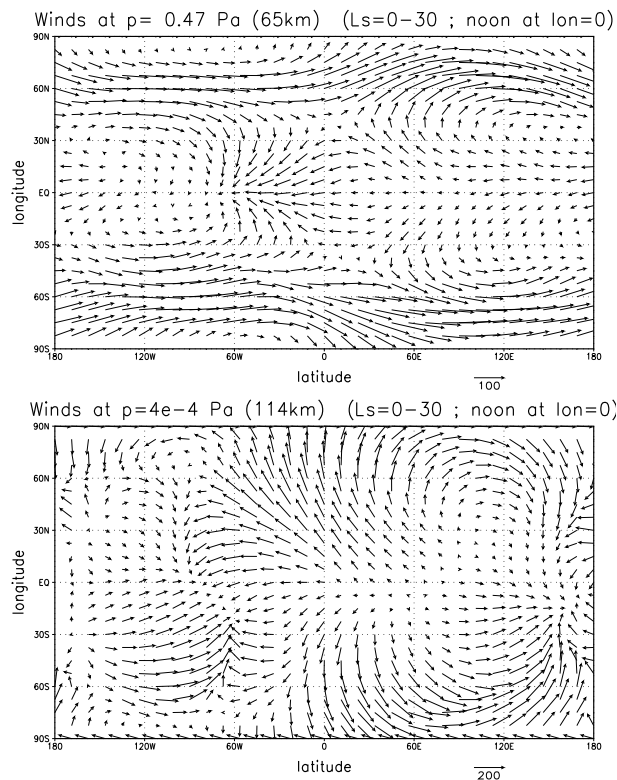Winds at p=4e−4 Pa (114km) (Ls=0−30 ; noon at lon=0)

Figure 3: Horizontal wind field simulated by the GCM near Northern spring equinox at two pressure levels. The structure of the wind around 60 km is characteristic of thermal tides propagating from the lower atmosphere as predicted by classical atmospheric tidal theory (Zurek, 1976). At higher altitude, solar to antisolar circulation forced by the NIR CO_2 absorption progressively dominate.

General Circulation of the upper atmosphere

Simulations were performed using 32 model layers starting at 5 m, 20 m, 50 m, 115 m, 240 m, 490 m, 980 m, etc... with the uppermost level at about 101, 106, 110, 114 and 120 km. The typical characteristic of the simulated atmosphere are shown on figure 2 and 3.

II. Comparison with observations

Comparison MGS radio-occultation

The MGS radio-occultation experiment (Hinson et al., 1999, 2001). provides high resolution profiles of atmospheric density, pressure, and temperature versus radius and geopotential between 0 and about 35 km. We have performed detailed comparison with the dataset obtained during the first year of the mapping mission, with a particular interest in the vertical structure of the lower atmosphere. Waves structures has not been analysed,
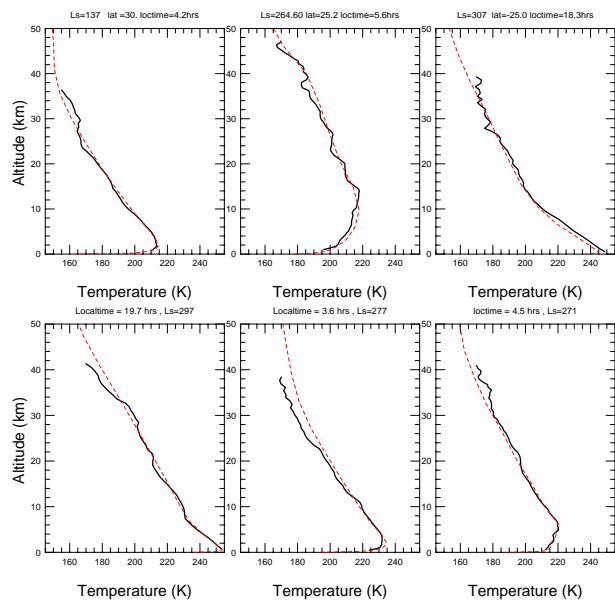

Figure 4: Example of very good fits to the observations that can be obtained with the MGS "dust scenario" at various seasons and local time in the tropics (top) and in the southern hemisphere (bottom) (Observation: black solid line ; Model: red dashed lines). Using this dust scenario, the model can usually well simulate the variations of the temperature profiles due to change in dust loading and insolation.

yet.

In general: very good agreement between model and observations. Using the "MGS dust scenario" (Fig. 1), the simulated temperature profiles are usually within 10K from the observations. Very often, the model is able to predict the detailed thermal structure of the atmosphere with a striking accuracy (Figure 4). This is true for various seasons and latitudes, corresponding to very different dust loading and insolation. Figure 4 bottom illustrates the ability of the model to simulate the diurnal changes in the lower atmosphere thermal structure as a function of local time for 3 profiles, here obtained during summer in the southern hemisphere. During southern summer, the low atmosphere thermal structure can be well reproduced by the model in spite of a large range of behavior. Interestingly, In a previous paper addressing the comparison of NASA Ames Mars GCM with this southern summer radioscience dataset, Joshi et al. (2000) noted that the model was not able to match such structures. In particular, this was the case for the temperature inversion peaking at 6 km shown on Figure 4, bottom right (see Fig. 3 in Joshi et al. 2000), leading them to suggest that water ice clouds, an non-uniform vertical distribution of the dust or enhanced gravity wave activity was necessary to explain the observations.
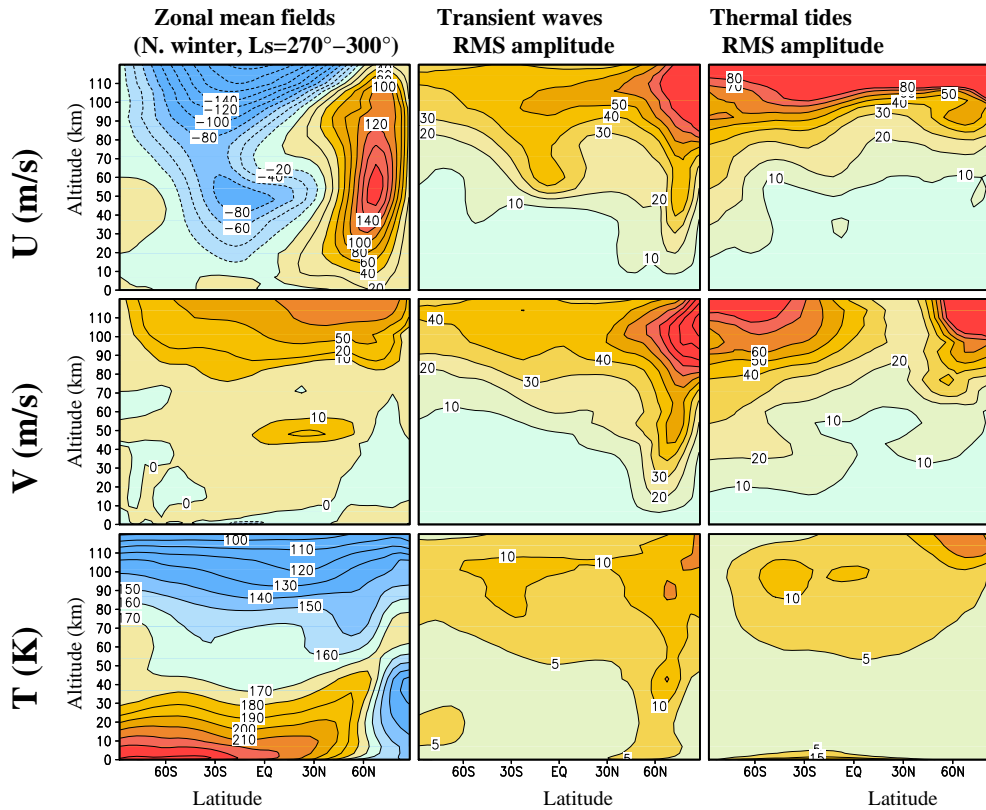
Figure 2: A summary of the dynamical fields simulated by the extended GCM during Northern winter ($L_s = 270^o - 300^o$). The middle and right columns illustrate that the atmospheric dynamic is especially rich above 70 km where very little data is available, and where Non-LTE processes must be taken into account. At every seasons, including this particular one, strong thermal tides (diurnal and semi-diurnal westward waves as well as a combination of non-migrating tides) are excited by the diurnal cycle near the surface as well as by the local diurnal heating by the CO_2 absorption of near infrared radiation. In addition, large amplitude transient waves are simulated above 80 km, with in particular wavenumer 1 Kelvin waves with a period of about 3 days. In this particular case (N. winter), the zonal mean circulation above 70 km is controlled by wave-mean flow interaction. The westward thermal tides are especially important. For instance, they drag the zonal mean wind toward retrograde (negative) values, creating a summer to winter hemisphere mean meridional circulation, and contributing to force a warming of the atmosphere above the winter pole. However, the zonal mean fields (column 1) are not representative of the mean circulation given the large diurnal variations (column 3).

Some problems, locally

Local variations in dust loading. During some seasons, the dust loading can be highly variable spatially and temporally. For instance, this is the case during summer in the southern hemisphere, leading to slight disagreement between observations and model, with modeled temperatures warmer or colder than the observations.

Low atmosphere in northern polar regions in summer. A small, systematic disagreement between the observations and the simulations of the low atmosphere thermal structure (< 5 km) is observed in the northern summer polar spectra (Figure 5). This could be due to non-realistic surface properties in the model (local ice) or, more likely, to the impact of water ice clouds.

Waves and inversions in the Northern summer sub-tropics. Among the profiles observed during northern summer in the sub-tropics are found profiles containing strong inversions (Figure 6). They are particularly found near pavonis Mons and Tharsis. These inversions are almost not reproduced by the model. Small "bumps" in the mean temperature profiles at altitude similar to the observed inversions can sometime be simulated, but the magnitude is much smaller than in reality (Figure 6). These inversions may results from dynamical phenomenons (tidal waves not well represented in the models, tidal waves interacting with subgrid-scale gravity waves) and/or the presence of water ice clouds.

Southern winter polar temperature. Figure 7 shows a subset of temperature profiles obtained around 70^oS latitude at various time during southern winter. Discrepencies between observations and models are obvious, especially toward the end of the winter when atmospheric temperature are getting warmer as the edge of the polar night receed toward the pole. Such differences are unexpected, although they may partly result from the fact that the database contains fields averaged over 30° Solar Longitude. Further work is required to better understand the disagreement between model and observations.

Comparison with the The MGS Thermal Emission Spectrometer temperature retrieval

Detailed comparison have been performed by the AOPP team, and will be presented in a companion paper.

Comparison with lander entry profiles

Figure 8 shows temperature measurement taken during the entry phases of the Viking landers (Seiff and Kirk, 1977) and Pathfinder (Magalhães et al., 1999) compared with MCD prediction at the same location and time for
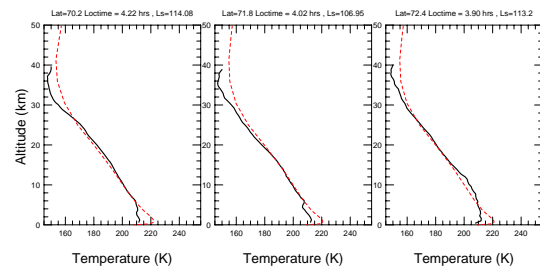

Figure 5: Examples of temperature profile comparison (Observations: black solid line ; GCM: red dashed lines) in the North Polar region in summer. Note the systematic disagreement observed in the low atmosphere.
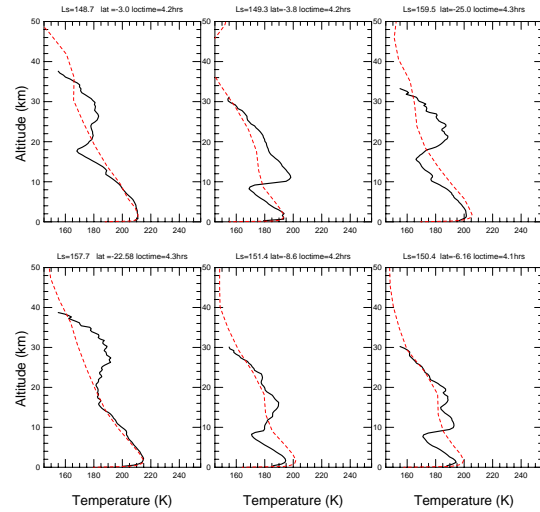

Figure 6: Six examples of radioscience profiles (solid black lines) from the northern summer tropics exhibiting strong temperature inversions which are not reproduced by the General Circulation Model (red dashed lines).
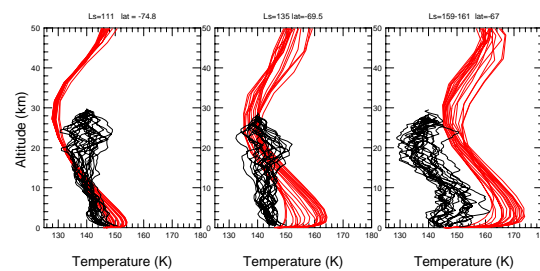

Figure 7: Three sets of 20 radio-science profiles (black) obtained in the south polar region in or near the polar night at different date, compared to sets of Mars GCM predictions (red) at the same time and location.
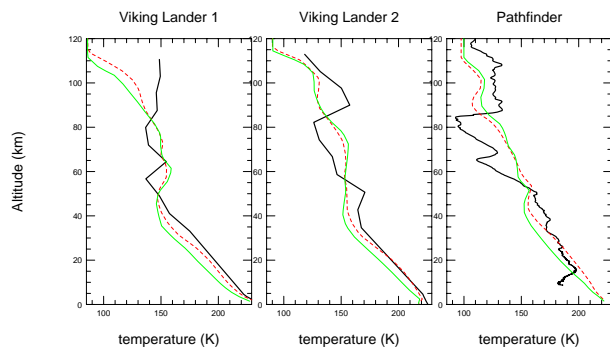
Figure 8: Entry Temperature profile (thick black line) observed in situ by the Viking and Pathfinder landers compared with GCM profiles retrieved from the Mars Climate database MGS dust scenario (green solid line) and a "dusty" scenario (red dashed line).

the MGS dust scenarios and for a simulation were the dust opacity has been overestimated (dash line) In the lower atmospere below 40 km, the three temperature profiles are at least 10 K warmer than our "best guess" MGS scenario. They are better matched by the dusty scenario, although for Viking 1 this is still not warm enough. These results are surprising since the "dusty" scenario profiles are almost always warmer than the radio-occultation profiles obtained at similar location and time. Could this be due to interranual variability ? In fact, the entry profiles appear more and more to be in conflict with remote observations obtained simultaneously (Clancy et al., 2000, Dave Hinson, personnal communication, 2001). This could be due to local effects and/or to some misunderstanding in the data analysis.

Comparison with upper atmosphere density aerobraking measurements

The GCM prediction of the density have been compared with the measurements of the density recorded ins-situ by MGS. This comparison, and the analysis of the waves involved in the observed structure are described in Angelats i Coll et al., this issue.

References

[Clancy et al., 2000] Clancy, R. T., Sandor, B. J., Woff, M. J., Christensen, P. R., Smith, M. D., Pearl, J. C., Conrath, B. J., and Wilson, R. J. (2000). An intercomparison of ground-based millimeter, MGS TES, and Viking atmospheric temperature measurements: Seasonal and interannual variability of temperatures and dust loading in the global Mars atmosphere. *J. Geophys. Res.*, 105:9553–9571.

[Forget et al., 1999] Forget, F., Hourdin, F., Fournier, R., Hourdin, C., Talagrand, O., Collins, M., Lewis, S. R., Read, P. L., and Huot,

J.-P. (1999). Improved general circulation models of the Martian atmosphere from the surface to above 80 km. *J. Geophys. Res.*, 104:24,155–24,176.

[Haberle and Jakosky, 1991] Haberle, R. M. and Jakosky, B. M. (1991). Atmospheric effects on the remote determination of thermal inertia of Mars. *Icarus*, 90:187–204.

[Hayashi et al., 1995] Hayashi, J. N., Jakosky, B. M., and Haberle, R. M. (1995). Atmospheric effects on the mapping of Martian thermal inertia and thermally derived albedo. *J. Geophys. Res.*, 100:5277–5284.

[Hinson, 2001] Hinson, D. (2001). Radio occultation measurements of forced atmospheric waves on Mars. *J. Geophys. Res.*, 106:1463–1480.

[Hinson et al., 1999] Hinson, D. P., Flasar, M., Simpson, R. A., Twicken, J. D., and Tyler, G. L. (1999). Initial results from radio occultation measurements with mars global surveyor. *J. Geophys. Res.*, 104:26,997–27,012.

[Joshi et al., 2000] Joshi, M., Haberle, R. M., Hollingsworth, J., and Hinson, D. (2000). A comparison of MGS phase 1 aerobraking radio occultation data and the NASA Ames Mars GCM. *J. Geophys. Res.*, 105:17,601–17615.

[Keating et al., 1998] Keating, G. M., W., B. S., and 29-coauthors. (1998). The structure of the upper atmosphere of mars: In situ accelerometer measurements from Mars Global Surveyor. *Science*, 279:1672–1676.

[Lewis et al., 1999] Lewis, S. R., Collins, M., Read, P. L., Forget, F., Hourdin, F., Fournier, R., Hourdin, C., Talagrand, O., and Huot., J.-P. (1999). A climate database for Mars. *J. Geophys. Res.*, 104:24,177–24,194.

[Lopez-Puertas and Lopez-Valverde, 1995] Lopez-Puertas, M. and Lopez-Valverde, M. (1995). Radiative energy balance of CO_2 non-LTE infrared emissions in the Martian atmosphere. *Icarus*, 114:113–129.

[Magalhães et al., 1999] Magalhães, J. A., Schofield, J. T., and Seiff, A. (1999). Results of the Mars Pathfinder atmospheric structure investigation. *J. Geophys. Res.*, 1999:8943–8956.

[Mellon et al., 2000] Mellon, M. T., Jakosky, B. M., Kieffer, H. H., and Christensen, P. R. (2000). High resolution thermal inertia mapping from the Mars Global Surveyor Thermal Emission Spectrometer. *Icarus*, 148:437–455.

[Paige et al., 1994] Paige, D. A., Bachman, J. E., and Keegan, K. D. (1994). Thermal and albedo mapping of the polar regions of Mars using Viking thermal mapper observations, 1, North polar region. *J. Geophys. Res.*, 99:25959–25991.

[Paige and Keegan, 1994] Paige, D. A. and Keegan, K. D. (1994). Thermal and albedo mapping of the polar regions of Mars, 2, South polar region. *J. Geophys. Res.*, 99:25993–26013.

[Pallucomi and Kieffer, 1981] Pallucomi, F. D. and Kieffer, H. H. (1981). Thermal inertia mapping of Mars from 60°S to 60°N. *Icarus*, 45:415–426.

[Seiff and Kirk, 1977] Seiff, A. and Kirk, D. B. (1977). Structure of the atmosphere of Mars in summer mid-latitudes. *J. Geophys. Res.*, 82:4364–4378.

[Wilson and Hamilton, 1996] Wilson, R. W. and Hamilton, K. (1996). Comprehensive model simulation of thermal tides in the Martian atmosphere. *J. Atmos. Sci.*, 53:1290–1326.